HHS Public Access
Author manuscript
J Am Chem Soc. Author manuscript; available in PMC 2020 September 11.

Published in final edited form as:
J Am Chem Soc. 2019 September 11; 141(36): 14005–14020. doi:10.1021/jacs.9b06222.

Biomedically Relevant Self-Assembled Metallacycles and Metallacages

Hajar Sepehrpour[a], **Wenxin Fu**[c], **Yan Sun**[a,b,*], **Peter. J. Stang**[a,*]

[a.]Department of Chemistry, University of Utah, 315 South 1400 East, Room 2020, Salt Lake City, Utah, 84112, United States

[b.]School of Chemistry and Chemical Engineering, Yangzhou University, Yangzhou, Jiangsu 225002, P. R. China

[c.]Beijing National Laboratory for Molecular Sciences, Institute of Chemistry, Chinese Academy of Sciences, Beijing 100190, China

Abstract

Diverse metal-organic complexes (MOCs), such as rectangles, triangles, hexagons, prisms and cages, can be formed by coordination between metal ions (Pt, Pd, Ru, Rh, Ir, Zn, Co and Cd) and organic ligands, providing applications as alternatives to conventional biomedical materials for therapeutic, sensing and imaging purposes. As anticancer drugs, MOCs have been investigated in the treatment of malignant tumors in the lung, cervical, breast, colon, liver, prostate, ovarian, brain, stomach, bone, skin, mouth, thyroid, and other malignancies. As drug carriers, MOCs with one, two and three cavities have been prepared for the loading and release of different drugs. In addition, MOCs can target proteins by the shape effect, and recognize sugars and DNA by electrostatic interactions, as well as estradiol by host–guest interactions, etc. This perspective mainly covers achievements in the biomedical application of MOCs. We aim to identify some key trends in the reported MOC structures in relation to their biomedical activity and potential applications.

Graphical Abstract

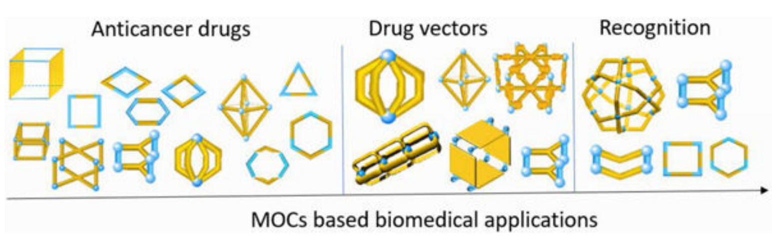

Keywords

Metallacycle; metallacage; metal-organic complexes (MOCs); biomedical application

*Corresponding Author sunyan@yzu.edu.cn, stang@chem.utah.edu.

1. Introduction

Metal-organic complexes (MOCs) [1, 2] are well-defined, discrete two-dimensional (2D) or three-dimensional (3D) molecular entities[3] with suitable metal centers undergoing coordination-driven self-assembly with ligands containing multiple binding sites. [4, 5] The inspiration[6] for using MOCs in biological applications[7–12] originates from their characteristic properties, such as the ease of fine-tuning the dimensions of the complexes, [13] the selection of metal ions with specific sizes, their coordination geometry, and the simple incorporation of essential functional groups through pre- or post-self-assembly[14–18] modifications (Scheme 1, **top**).

By using Pt, Pd, Ru, Rh and Ir as the metal center (Scheme 1, **bottom, right**), Therrien, [7, 8] Stang, [19] and Casini [9] published recent work on MOC design for biochemical and biomedical applications (Scheme 1, **bottom, middle**). For example, 2D metallacycles such as triangles, [21] rectangles, [22] rhomboids [23] and hexagons [24] can be formed by the coordination between the ligands and a metal acceptor for biomedical applications. 3D metallaprisms can be prepared by [2+3] assembly between 1, 3, 5-substituted triazine and Ru-,[25] Rh-,[26] or Ir-[26]-containing organic ligands, which are mainly used as drug delivery vectors. Furthermore, Pt metallacages, which are used as both anticancer drugs and drug carriers, can be formed by the [2+4+8], [2+6+12] assembly of tetra-(4-pyridylphenyl)-ethylene (TPPE), [27] porphyrin, [28] and hexakis[4-(4′-pyridylethynyl) phenyl]benzene (HPPB) [29] (used as faces), dicarboxylate moieties (used as pillars), and *cis*-$(PEt_3)_2Pt(OTf)_2$ (used as corners). In addition to metallaprisms and metallacages, metallacapsules [30] can be formed by the [2+4] assembly of metal ions and organic donor ligands.

Biological studies involving MOCs are widely conducted[19] (Scheme 1, **bottom, left**), and the effect of the characteristic structural features of MOCs is described. [20] For example, Therrien and coworker [7, 8] found that half-sandwich Ru complexes are essential functional units in treating many kinds of cancers. In contrast to Therrien's work, our group has devoted much attention to Pt-containing MOCs and their in vivo study. [23, 27–29] We introduced various functional units, such as TPPE, into MOCs, improving the precision of cell imaging and achieving "tissue-specific" aggregation and imaging.[31] We integrated chemotherapy with photodynamic therapy (PDT) into a single platform, achieving a synergistic anticancer effect and demonstrating that this combination of tumor treatments effectively prolonged mice survival. [21] We also prepared three porphyrin based metallacages. [28] By tuning the metal ions in the porphyrin ring, we realized multimodal three-state imaging with magnetic resonance imaging (MRI), positron emission tomography (PET) and near-infrared fluorescence imaging (NIRFI). [28] Moreover, we imbedded MOCs into target-specific polymeric nanoparticles, resulting in the successful combination of the therapeutic and diagnostic properties of these structures and improving the theranostic outcome. Thus, accurate diagnosis of disease location and precision treatment were achieved. [28]

MOCs can be used to alleviate the toxicity, degradation and resistance issues of anticancer drugs.[11] Crowley[32] and Casini[33] designed various metallacapsules as vectors. Yam[34] synthesized rectangles used as vectors for delivering Pt, Pd, and Au-containing guests.

Crowley developed metallacapsules with two and three cavities, which can be used as carriers for loading and releasing two kinds of guests (cisplatin and triflate).[35] In addition, metallaprisms, [36] metallabarrels, [37] and metallacages[38] are used as carriers for drug delivery.

Various drugs, such as cisplatin, [39] porphin, [25] and Ru-containing guests, [40] can be encapsulated into these cavities. Lippard and Zheng reported prodrug-containing MOCs as another kind of drug delivery vector[41] and prepared both metallacycles[42] and metallacages[43] for drug delivery.

Furthermore, biomolecules such as proteins, [44–46] sucrose, [47] hormones, [48] and DNA[49–50] can be recognized by MOCs through shape effects, electrostatic and host–guest interactions. In this perspective, we describe recent achievements in the design of MOCs with anticancer properties and recognition of biomolecules, as well as their potential as drug delivery vectors for therapeutic or imaging purposes. Current challenges and future directions on this topic are also discussed.

2. MOCs as Anticancer Agents

To date, MOCs have been used in the treatment of malignant tumors in the lung, [51] cervical, [52] breast, [53] colon, [54] liver, [55] prostate, [56] ovarian, [57] brain, [58] stomach, [59] bone, [60] skin, [61] mouth, [61] thyroid, [62] blood[63] and so on (Scheme 2A). The anticancer effect of MOCs is achieved mainly through inducing membrane damage, [61] cell apoptosis[64] and autophagy, [67, 69] DNA damage, [65] and increased p53[66] expression (Scheme 2B). As shown in Scheme 2C, apoptosis accounts for the majority of effect for MOC-mediated anticancer activity. As shown in Scheme 3A, MOC-based drugs have two main use strategies. The first is to use them directly as drugs. The second is to use MOCs as coassembly units to form MOC based nanoparticles (MNPs) and to then use the MNPs as therapeutic drugs (Scheme 3B). Both MOCs and MNPs exhibit better cell internalization behaviors than their precursors due to their enhanced permeability and retention (EPR) effect (Scheme 2C); moreover, the targeting of drugs to tumors is enhanced because of the introduction of functional units such as biologically specific sequences. [68]

The action of MOC-based anticancer drug progresses through three stages (Scheme 3D). In the first stage (Scheme 3D, I), most MOCs enter tumor tissues by the size effect and then enter cells by interaction between the positive charges and the negative charges on the membrane.[69–70] In the second stage, the shape match (Scheme 3D, II) [60] between MOCs and DNA as well as the EPR effect work together. Recently, functional groups for reactive oxygen species (ROS) generation and cell imaging were also integrated into MOCs, [23] initiating the combination of chemotherapy and PDT and improving the treatment outcome (Scheme 3D, III). For these MOCs, mitochondria are another major target organelle (Scheme 3C).

Some activity focus on the MOCs-related organ-specific activity, as summarized in Figure 1. The heterometallic Ru–Re metallacycle MOC **1** (Figure 1a) [53] was reported by Thomas; it functions as an intracellular singlet oxygen sensitizer that causes plasma membrane damage. Another heterometallic Ru–Pt metallacycle, MOC **2**, [23] was synthesized by our group and exhibits near-infrared emission, strong two-photon absorption (TPA), and high $^1O_2$ generation efficiency. MOC **2** accumulates in mitochondria because of the negative potential difference across the mitochondrial membrane. Elevated intracellular ROS levels within mitochondria can trigger caspase activation and apoptosis. MOC **2** partially accumulates in the nucleus in addition to mitochondria. The in vivo two-photon PDT efficacy of MOC **2** was investigated using A549 tumor-bearing nude mice with a xenograft tumor volume of 80 mm^3. In the treatment group, the tumors shrank gradually and were reduced to 78% of the original size on day 14, while the tumors in the control group showed more than a 13-fold growth over the same period. No noticeable body weight loss was found during the treatment process, indicating the minimal side effects of MOC **2**. Representative images of A549 tumors in mice with these different treatments are shown in Figure 1b.

In addition to Ru(II) complexes, porphyrin is another important photosensitizer. Yao designed amphiphilic organoplatinum(II), MOCs **3, 4** (Figure 1c), [22] with a porphyrin unit as the core and hydrophilic glycol units as the tail. The cellular uptake of MOCs **3, 4** by A549 cells was investigated. Intracellular uptake and in vitro cytotoxicity assays confirmed that MOC **3, 4** micelles exhibited markedly enhanced cellular uptake and antitumor efficacy. Boron dipyrromethene (BODIPY) dyes are the third kind of functional unit in PDT. Huang and Cook designed two Pt(II) triangles, MOCs **5, 6** (Figure 1d), [21] that contain a pyridyl-functionalized BODIPY ligand, in which the platinum acceptors are toxic chemotherapeutics and the BODIPY donor is an imaging probe and photosensitizer. In vitro studies demonstrated that MOCs **5, 6** improved their anticancer efficacy, and the combination of PDT and chemotherapy showed excellent synergistic effects against HeLa cells. In addition to the properties of BODIPY in PDT, its high fluorescence quantum yield is another important characteristic, making BODIPY-containing complexes good candidates for fluorescence imaging. For example, Lee reported four BODIPY-containing palladium triangles/squares, MOCs **7–10** (Figure 1e),[58] which were more cytotoxic to brain cancer (glioblastoma) cells than to normal fibroblasts. The characteristic green fluorescence of the BODIPY ligands permitted their intracellular visualization using confocal microscopy, demonstrating that the compounds were localized in the cytoplasm and on the plasma membrane. The cytotoxicity of these MOCs to glioblastoma cells was higher than that of a benchmark metal-based chemotherapeutic drug, cisplatin. Conventional fluorophores often exhibit an undesirable aggregation-caused quenching (ACQ) effect, wherein aggregation-induced emission (AIE)-active fluorophores emit bright fluorescence in the aggregate state via the restriction of intramolecular motion. Thus, the fluorescent polymer rhomboidal Pt(II) metallacycle MOC **11** (Figure 1f), [31] containing TPE, was designed and was used in cell imaging, showing a significant enrichment in lung cells. We also designed the highly fluorescent MOC **12**, [68] in which the TPE-based bipyridyl ligands are the donors and act as a spectroscopic handle for live cell imaging, while the acceptor PhenPt units are employed as an anticancer drug.

Further self-assembled nanoparticles and vesicles were prepared from MOC **12**, and effects of the morphology and size of these assemblies on the endocytic pathways, uptake rates, internalization amounts, and cytotoxicities were found. Therrien prepared a series of arene ruthenium metallacycles containing long alkyl chains, which increase the lipophilicity and molecular weight of the metallacycles to better target the EPR effect.

As shown in Figure 1g, Therrien and coworkers designed metallarectangles, MOCs **13**, **14**, [57] which are highly potent towards human ovarian cancer cells while displaying pronounced selectivity for cancer cells over healthy cells. Very recently, an NIR-II theranostic nanoprobe incorporating the Pt(II) MOC **15** (Figure 1h) was reported. [55] The nanoprobe was found to accurately diagnose cancer with high resolution and selectively deliver MOC **15** to tumor regions via the EPR effect.

In vivo studies revealed that nanoprobes efficiently inhibit the growth of tumors with minimal side effects. In addition to studies on malignant tumors in the brain, cervical, lung, ovarian, and liver, studies have been conducted. Yoshizawa prepared MOCs **16**, **17** (Figure 1i), [63] which showed higher anticancer activities (up to 5-fold) against human leukemic cells and even higher activities (up to 125-fold) against cisplatin-resistant cells than cisplatin. Moreover, the anticancer cytotoxicity of MOCs **16**, **17** is highly selective—these complexes are approximately 10 times more toxic to cancer cells than to nonmalignant cells.

In addition to organ-specific activity, several MOCs also show activity in different types of tumors (Figures 2, 3). We prepared three porphyrin-based metallacages, MOCs **18–20** (Figure 2a), [28] for the fabrication of MNPs, and then studied their antitumor activity against U87MG cells and A2780cis cells. By combining NIRFI, PET, and MRI, we obtained precise detection as well as therapy for some tumors. The simultaneous use of highly sensitive and high-resolution multimodal imaging methods helps to overcome the limitations of each modality alone and offers complementary and accurate insight into tumor characteristics (Figure 2b). The combination of chemotherapy and PDT effectively ablated all tumors (A2780CIS cells) in mice without recurrence during the course of the therapy. PDT eliminated the primary tumor tissue through local irradiation, and the chemotherapeutic drug killed the residual cancer cells, thus effectively inhibiting tumor recurrence. Gene expression analysis of tumors confirmed the distinct alteration pattern of genes in response to different therapeutic modalities. Similar to the work described above, another study focused on MOC **21** (Figure 2c) as a component of theranostic supramolecular MNPs. [27] In vivo investigations demonstrated that **MOC 21-**based MNPs possess higher antitumor efficacy with lower toxicity than free platinum anticancer drugs (oxaliplatin, carboplatin, and cisplatin).

Therrien et al. focused on the design and synthesis of Ru-containing MOCs, as shown in Figure 2d. The cytotoxicity of MOCs **22**, **23** was evaluated against cancer (MCF-7, B16F10, A549) and nonmalignant cells. MOC **22**, **23** also showed higher cytotoxicity to cancer cells than to normal cells. [64] Lippard and Zheng designed a hexanuclear platinum metallacage (Pt_6L_4), MOC **24** (Figure 2e), which is taken up in high amounts by cancer cells. [65] Biophysical analysis confirmed that MOC **24** noncovalently interacts with DNA.

In addition to platinum(II) and ruthenium(II) MOCs, palladium(II) MOCs exhibit anticancer activity. Crowley synthesized a series of $[Pd_2(L)_4](BF_4)_4$ MOCs, MOCs **25–28** (Figure 2f–g). [30] Investigations with MOC **27** revealed that it induced cell death within minutes. As shown in Figure 3h, Casini prepared a series of similar structures, [51] which exhibit higher cytotoxicity inall tested cancer cells than cisplatin. We designed rhomboidal Pt(II) metallacycles, MOCs **33**, **34** (Figure 3i), [52] and investigated their antitumor activity in HeLa and A549 cells, where they inhibited tumor growth. Chi et al. designed two tetracationic heterobimetallacycles, MOCs **35**, **36** (Figure 3j), [62] and explored the potential biological effects of these systems. The cytotoxic effects of both of these new complexes against the cancerous cell lines were reported.

Much of the antitumor activity of MOCs is due to the inherent properties of transition metal complexes, and the EPR effect. Terenzi reported size- and shape-related anticancer performances.

As shown in Figure 2k, he and coworkers synthesized Pt(II) quadrangular boxes, MOCs **37–39**, [60] and found three Pt molecular squares of distinct size that showed biological activity against cancer cells that heavily influenced the expression of genes known to form guanine quadruplexes (G-quadruplexes) in their promoter regions. Three cancer cell lines (U2OS, VM-1 and MCF-7) were treated, and MOCs **37–39** reduced cell viability in most of the tested models. The DNA binding activity and the in vitro effect on cancer cells can be modulated with Pt MOCs according to the size and shape of the complex (Scheme 3D, II).

Das and coworkers reported a series of findings on MOC-related antitumor activity. As shown in Figure 3a, MOCs **40**, **41**, [61] were synthesized, and the results of cell cycle analysis and live propidium iodide staining suggested that they induced a loss of membrane integrity that might ultimately lead to necrotic cell death. Furthermore, two nanoscale supramolecular metallacycles, MOCs **42**, **43** (Figure 3b–c), were also synthesized by Das.[24] Relatively higher apoptosis induction was observed in A549 cells treated with MOCs **42**, **43** than in those treated with cisplatin, confirming the induction of apoptotic death in A549 cancer cells by MOCs **42**, **43**. In addition, Das and coworkers also designed MOCs **44**, **45** (Figure 3d) and evaluated the growth inhibitory effects of these complexes against HT-29 colorectal adenocarcinoma cells and MCF-7 and MDA-MB-231 breast cancer cells. [54] The structure of MOCs **44**, **45** improved the cytotoxic effects against both types of cancer cells.

Chi and coworkers devoted substantial attention to digestive tumor (gastric cancer, colorectal cancer, and liver cancer) treatments. As shown in Figure 3f, this group synthesized large molecular metallarectangles, MOCs **46, 47**, [59] and determined the cytotoxicity of these MOCs in the SK-hep-1 (liver cancer), AGS (gastric cancer), and HCT-15 (colorectal cancer) human cancer cell lines. Subsequently, they designed cobalt–ruthenium heterometallic molecular rectangles, MOCs **48–50** (Figure 3f), which showed marked inhibitory activity against AGS cells. [67] These findings suggest that MOCs **48–50** induce autophagy and apoptosis in gastric cancer cell lines and can be considered potential drugs for the treatment of gastric cancer. The metallabowl complex MOC **51** (Figure 3g) also inhibited the growth of human digestive cancer cell lines. [66] Exposure to 2 μM MOC **51** increased the expression of APC mRNA 2.9-fold, and p53 mRNA expression in HCT116 cells treated with 2 μM MOC **51** increased 4.1-fold relative to that in untreated controls, a statistically significant increase. Additionally, Chi designed MOCs **52**, **53** (Figure 3g), [69] inducing autophagic activity in HCT-15 cells. These results suggest that the autophagic response elicited by

MOCs **52**, **53** could mediate the anticancer effects observed in human colorectal cancer cells. As a part of the Ru MOC-related work, MOCs **54–56** (Figure 3h) were also synthesized;[71] these complexes exhibited good anticancer activity in all tested cancer cell lines (HCT-116, MDA-MB-231, MCF-7, HeLa, A549, and HepG-2). Furthermore, these results suggest that the complexes likely interact with ctDNA via an electrostatic binding mode, which is often caused by the interaction between positively charged drug molecules and negatively charged phosphoric moieties in the DNA.

Therrien designed six pentamethylcyclopentadienyl Rh(III) and Ir(III) metallarectangles, MOCs **57–62** (Figure 3i). [56] The antiproliferative activity of these tetranuclear complexes was evaluated *in vitro* in cancer (DU-145, A-549, HeLa) and nonmalignant (HEK-293) cell lines. Mitochondrial aggregation was reported to occur when the cells entered apoptosis and accordingly led to the release of cytochrome c into the cytosol, which in turn triggered the apoptotic cascade. Lee designed BODIPY-based Ru(II) and Ir(III) metallarectangles, MOCs **63–66** (Figure 3j). [70] MOCs **64–66** show predominantly cytoplasmic modes of action, but these complexes also significantly interact with genomic DNA. Four octanuclear Ru(II) cages, MOCs **67–70** (Figure 3k), [72] were synthesized by Mukherjee et. al. MOC **69** and MOC **70** possess excellent anticancer activity, with the lowest IC_{50} values among cancer cell lines against both A549 and HeLa cell lines. The active of these octanuclear cages contain polyaromatic rings suggesting that the nature and sometimes the number of aromatic rings in the acceptor unit may improve the anticancer activity of the cages.

3. MOCs as Drug Delivery Systems

Crowley designed $[Pd_2L_4](X)_4$ cages, MOCs **71–72** (Figure 4a), [32] which enable the encapsulation of two cisplatin molecules within the metallosupramolecular architecture through hydrogen bond interactions between the cage and the amine ligands of the cisplatin guest. MOCs **71–72** can be reversibly disassembled/reassembled in a controlled stimuli-responsive manner by the addition and subsequent removal of competing ligands.

Casini and Kuhn reported a series of exofunctionalized self-assembled Pd_2L_4 cages, MOCs **73–76** (Figure 4b). [73] Among these MOCs, only MOC **75** exhibited increased toxicity to SKOV-3 cells. The anticancer activity of the host–guest complex (MOC **75**/cisplatin) was studied in SKOV-3 human ovarian carcinoma cells and exhibited an approximately tenfold enhanced toxic effect in cancer cells compared to the effect of cisplatin and MOC **75** alone. Within the framework of designing new self-assembled metallosupramolecular architectures for drug delivery, seven $[Pd_2L_4]$ cages MOCs **77–83**[33] featuring different groups in the exo position were synthesized (Figure 4c). Encapsulation of the anticancer drug cisplatin in selected cages has been studied by nuclear magnetic resonance (NMR) spectroscopy, and the results show that if the polarity of the solvent is sufficient, the metallodrug can easily be encapsulated in the hydrophobic cavity of the cage. Aiming to develop functional metallosupramolecular drug delivery vectors, Casini synthesized Pd_2L_4 cages, MOCs **84–87**, [39] conjugated to four integrin ligands with different binding affinities and selectivities (Figure 4d) to solve the problem of metallodrug speciation. Upon encapsulation, cisplatin showed increased cytotoxicity in vitro.

A series of multiaddressable platinum(II) molecular rectangles, MOCs **88–91** (Figure 4e–h),[34] with different rigidities and cavity sizes, were synthesized by Yam. The introduction of pH-responsive functionalities to the ligand backbone generates multifunctional molecular rectangles that exhibit reversible guest release and capture upon the addition of acids and bases, indicating the potential of these complexes to control the delivery of therapeutics upon pH modulation. The synthesis of M_2L_4 (M = Pd, Pt) molecular cages, MOCs **92–94** (Figure 4i),[74] was reported by Casini and Kuhn. MOCs **92–94** were demonstrated to encapsulate the anticancer drug cisplatin. Both host–guest systems show a higher cytotoxic effect in A549 cells than either cisplatin or MOCs **92–94** alone.

Crowley reported the first example of a triple cavity $[Pd_4(L)_4]^{8+}$ cage, MOC **95** (Figure 4j),[35] the central cavity of which differs from the peripheral cavities in that it is phenyl-linked rather than having a pyridyl core. The difference in the cavity character results in selective binding of the cisplatin guest in the peripheral cavities, with triflate binding within the central cavity and on the exohedral faces of the peripheral palladium(II) ions. All cavities could be simultaneously filled by introducing both cisplatin and triflate concurrently, providing the first example of a discrete metallosupramolecular architecture with segregated guest binding in differently designed internal cavities.

In addition to cisplatin, guests (Figure 5a), including porphin (**G2**),[25–26] coronene (**G3**),[36] pyrenyl-arene ruthenium complexes (**G4–6**),[40] pyrenyl nucleoside derivatives (**G7–12**),[75] porphin derivatives (**G13**),[29] curcumin (Cur, **G14**),[76] and 5-fluorouracil porphin (5-FU, **G15**),[38] can be delivered by **MOC**s **96–100**. As shown in Figure 5b, Therrien demonstrated that the metallacage MOC **97**[75] can carry and intracellularly deliver the photosensitizer **G2** following uptake by cells. The uptake and release of **G2** after internalization of the host −guest systems have been studied in various human cancer cells, such as A2780, HeLa, and A549 cells. The system displays hypochromic properties towards the photosensitizer loaded inside the cavity of the cage, resulting in the absence of extracellular phototoxic effects. As an extension to previous work, MOCs **99–100**[26] (Figure 5b) were synthesized, and excellent phototoxicity was observed for these two host–guest systems. Only nanomolar concentrations of these systems were necessary to inhibit cell growth by photoactivation (20 J/cm^2). Half-sandwich structures are widely used for delivering many guests. For example, Therrien generated the carceplex system $[(\mathbf{G3})\subset$MOC $\mathbf{98}]^{6+}$.[36] Electrochemical investigation revealed the potential of metallaprisms to act as multielectron reservoirs and the ability of guest molecules to provide redox stability to metallaprisms. Additionally, Therrien synthesized three pyrenyl-arene ruthenium complexes as guests (**G4-G6** ⊂MOC **96**).[40] The antitumor activity of **G4-G6** and the corresponding host–guest systems were evaluated in vitro in different human cancer cell lines. All host–guest systems showed good anticancer activity, with IC_{50} values ranging from 2 to 8 μM after 72 h of exposure. The cytotoxicity of **G5** was at least 10 times higher than that of the reference compound $[Ru(\eta^6$-*p*-cymene)Cl_2(pta)] (RAPTA-C), while the **G5** system was 50 times more cytotoxic than RAPTA-C. In addition, Therrien synthesized six monosubstituted pyrenyl nucleosides and used them as guests. The carceplex nature of $[(\mathbf{G7–12}) \subset$ MOC $\mathbf{96/97}]^{6+}$was studied in solution by NMR techniques.[75]

We synthesized a discrete organoplatinum(II) metallacage, MOC **101** (Figure 5c–d), [29] which contains a platinum-based anticancer drug, and used it to encapsulate a photosensitizer [octaethylporphine (OEP), **G13**) [29] through noncovalent interactions. The host–guest complex was further encapsulated in an amphiphilic copolymer, resulting in the formation of MNPs that could codeliver a chemotherapeutic agent and a photosensitizer. The targeting ligand was introduced, endowing the formed MNPs with the ability to specifically deliver *cis*-$(PEt_3)_2Pt(OTf)_2$ (cPt) and **G13** to cancer cells overexpressing αvβ3 integrin. The MNPs accumulated greatly at tumor sites. In vivo studies demonstrated that MNPs exhibited superior antitumor activity in a drug-resistant tumor model by combining chemotherapy and PDT.

In addition to cisplatin and porphin, Cur (**G14**) is another anticancer drug that can be encapsulated. We prepared a host–guest complex comprising MOC **102** (Figure 5e)[76] and cucurbituril [8] (CB[8]), which acts as an aqueous carrier of Cur and delivers it to cancer cells. This work shows how a judicious combination of coordination-driven self-assembly and host–guest interactions can be utilized for hydrophobic drug delivery with improved efficacy. Mukherjee reported the synthesis of a water-soluble tetragonal molecular nanobarrel, MOC **103** (Figure 5f). [37] The hydrophobic cavity of MOC **103** was found to encapsulate hydrophobic **G14**. Such encapsulation makes hydrophobic **G14** highly soluble in water at room temperature in the presence of the barrel. In addition to the enhanced solubility of **G14** upon encapsulation, the panel-shaped aromatic walls of the barrel stabilize and protect the highly photosensitive **G14** from photodegradation under sunlight/UV irradiation. M_4L_4-type tetrahedral cage, MOC **104** (Figure 5g), was synthesized, [38] and its interactions with the anticancer drug 5-FU (**G15**) were investigated.[38] The cage's size and window are important for host–guest binding.

Hunter and Ward reported a range of organic molecules with acidic or basic groups that exhibit strong pH-dependent binding inside the cavity of a polyhedral coordination cage, MOC **105** (Figure 5h). [77] Guest binding in aqueous solution is dominated by a hydrophobic contribution, which is compensated by stronger solvation when the guests become cationic (by protonation) or anionic (by deprotonation). pH-dependent binding was observed for a range of guests with different functional groups (primary and tertiary amines, pyridine, imidazole and carboxylic acids) so that the pH-range can be tuned anywhere in the scope of 3.5–11. Among the MOCs, **106** has the largest overall (Figure 5i) [78] peripheral diameter of 5.4 nm and an internal cavity of 2.7 nm. After treatment with supercritical CO_2, a single crystal sample of MOC **106** transformed into amorphous material with the retention of the cage skeleton, which demonstrated good adsorption properties towards a small drug molecule, ibuprofen (Ibu, **G16**). [78] An Ibu release experiment in phosphate-buffered saline solution (pH 7.4) revealed that MOC **106** exhibited slow drug release behavior.

Lippard and Zheng presented a strategy that facilitates the delivery of multiple, specific payloads of Pt(IV) prodrugs using a well-defined supramolecular system. This delivery system comprises a hexanuclear Pt(II) cage, MOC **107** (Figure 5j), [43] that can host four Pt(IV) prodrug guest molecules. Also, Zheng used MOC **24** (Figure 5k) to encapsulate anticancer agents for delivery. [41] Using an anionic block copolymer, Zheng further formulated the host–guest complex into nanoparticles via electrostatic interactions. The resultant negatively charged nanoparticles have a size of approximately 80 nm, and can slowly release their therapeutic content and show efficacy comparable with that of cisplatin in vitro. Unlike the conventional MOC-based drug delivery platforms that were developed solely based on the intrinsic properties of MOCs, this work serves as a proof-of-concept to demonstrate the use of nanoformulations to fine-tune the properties of MOCs for drug delivery. Furthermore, Zheng presented another strategy to engage coordination-driven self-assembly for platinum drug delivery. The self-assembled supramolecular hexagon MOC **108** (Figure 5l) [42] is conjugated with three equivalents of Pt(IV) prodrugs and displays a therapeutic index superior to that of cisplatin against a panel of human cancer cell lines. They found that such complexes have superior therapeutic properties, including submillimolar potency against various human cancer cell lines and low cross resistance with cisplatin.

4. MOCs as Recognition Cavities

MOCs can target proteins by the exo-functionalization shape effect of MOCs, and thereby recognize protein, sugars and DNA by electrostatic interactions, as well as recognize L-dopa, D-penicillamine, D-sucrose and estradiol by host–guest interactions (Figure 6a). Fujita designed a dual-functionalized $M_{12}L_{24}$ sphere, **MOC 109** (Figure 6b), [44] bearing both titania-specific peptide aptamers and protein recognition sites. The selective recognition of titania surfaces was achieved by ligands with hexapeptide aptamers, whose fixation ability was enhanced by the accumulation effect on the surface of the $M_{12}L_{24}$ spheres. Chi reported studies of the protein interactions of the Ru-based MOC **110** (Figure 6c), [45] which can bind to the enhanced green fluorescent protein (EGFP) variant of GFP. The fluorescence emitted by the GFP protein was found to be completely quenched after a 6-h incubation of bacterial cells with MOC **110**, indicating that this metallacycle induces conformational changes in EGFP, disrupting the tripeptide chromophore. In addition to EGFP, some human proteins are targets of the arene ruthenium MOCs **96–98**.[46] Electrostatic interactions that induce the precipitation of these proteins seem to be the primary mode of interaction. In these particular cases, the metallaprisms induce severe changes in the secondary structure of the proteins. Additionally, Therrien studied the interactions between MOCs **96–98** and DNA decamers. A common feature of MOCs **96–98** is their inertness towards the pyrimidine nucleotides dCMP and dTMP but distinct reactivity with the purine nucleotides dAMP and dGMP. The interactions between DNA/RNA and platinum containing MOCs were studied by Sleiman and coworkers, who designed platinum squares, MOCs **111–114** (Figure 6d),[50] and examined their binding to DNA and RNA G-quadruplexes, including telomere-associated DNA and RNA sequences as well as oncogene sequences. These squares showed submicromolar binding affinities to telomeric repeat-containing RNA (TERRA), which regulates telomere elongation in both telomerase-positive and telomerase-negative (ALT) cancer cells.

In addition to proteins and DNA, D-sucrose can be recognized by MOCs. MOC **16** was used to selectively encapsulate D-sucrose in water from natural disaccharide mixtures within a nonfunctionalized polyaromatic cavity. MOC **16** binds D-sucrose with perfect selectivity through a combination of shape-complementary and specific CH-π (polyaromatic ring) interactions. [47] These results expand the versatility and utility of artificial polyaromatic nanospaces for the selective recognition and isolation of complex biomolecules in water. In addition to monosaccharides, polysaccharides can be detected by **MOCs**. For example, Yang designed a metallacycle, MOC **115** (Figure 6e), [79] and reported its application for heparin detection.

Chiral NH functionality-based discrimination is a key feature of nature's chemical armory, yet selective binding of biologically active molecules in synthetic systems with high enantioselectivity poses significant challenges. Cui reported the synthesis of MOC **116** (Figure 6f). [80] The low detection concentration and the high quenching constant for L-dopa and D-penicillamine drugs reveal that MOC **116** is an excellent chiral biosensor for the sensitive and selective detection of bioactive molecules. Hormones are another class of biomolecules that can be recognized by MOCs. Mirkin designed the Pt(II)-containing biomimetic molecular receptor MOC **117** (Figure 6g) [48] with an allosterically regulated nanoscale binding cavity capable of encapsulating large bioactive molecules. By modulating the coordination environment of the Pt(II) metal center, the molecular receptor is transformed from a rigid, cationic configuration to a flexible, neutral configuration, enabling the switching of the binding selectivity and the reversible encapsulation of large bioactive molecules.

5. Bacteria-/Virus-related and other Applications of MOCs

Our group reported that the rod-like tobacco mosaic virus (TMV), which has a negatively charged surface, can be assembled into 3D micrometer-sized, bundle-like superstructures via multiple electrostatic interactions with a positively charged molecular "glue" (MOC **118**, Figure 6h). [81] Due to the nanoconfinement effect in the resultant TMV/MOC **118** complexes and the AIE activity of the TPE units, these hierarchical architectures result in a dramatic fluorescence enhancement that not only provides evidence for the formation of novel metal −organic biohybrid materials but also represents an alternative to turn-on fluorescence. Li designed and assembled a 2D multilayered concentric supramolecular architecture, MOC **119** (Figure 6i), [82] which exhibited high antimicrobial activity against the gram-positive methicillin-resistant *Staphylococcus aureus* (MRSA) bacterium and negligible toxicity to eukaryotic cells. Furthermore, Fe(II) and Zn(II) helicates shows anti-bacterial activity.[83–85]

MOC related material with controllable nanostructures can be prepared by a well-established method, representing a new strategy for MNPs preparation.[86–88] Strategies toward the enhanced permeability and retention effect by increasing the molecular weight of MOCs,[89] enhanced kinetic stability of MOCs through ligand substitution, [90] bio conjugation strategies to modify MOCs with peptides for biomedical application are on the way. [91] As an important part of MOCs biological application, is how to confirm the precise mode of interaction between MOCs based anticancer drugs with DNA. [92] Very recently, Yang prepared the MOCs for selective therapy of cancers with controllable $^1O_2$ release. [93] Furthermore, enzyme-mimetic metallacages offers the possibility of MOCs related bionics application.[94]

6. Perspectives and Challenges

Exploration of the utility of these MOCs for various applications is still ongoing. By adjusting the chemical properties of the individual building blocks and the geometry of their linkages, diverse materials with fascinating biomedical properties can be generated. Thus, the best way to manipulate the properties of MOCs and overcome the current limitations is to increase the focus on basic structural construction, including the introduction of various metal ions with diverse directionality and the integration of multifunctional ligands, to create attractive MOCs with various topologies.

We have described Pt-containing MOCs as promising materials for biomedical applications. Usually, MOCs containing TPE are used for imaging, MOCs containing porphyrin and Ru(II) complexes are used for PDT, and MOCs containing BODIPY are used for both imaging and PDT. By in vivo investigations with the relevant MOCs, we integrated diagnosis and treatment in a single platform, introduced ROS-generating units into MOCs, and found that the synergistic effect of PDT and chemotherapy improved the efficacy of MOC-based drugs. Examples emphasizing the relationship between individual functional groups and the resultant effects are being established. For example, interchanging atoms (such as Mn and Cu in MOCs **18–20**) can completely alter the imaging properties of metallacages; although the construction of such types of MOCs is still in the initial stage, the design and investigation of these structures is quickly growing with continuous expansion of the related structural library.

Beyond simplifying the metal ions and ligands, the understanding of the relationships between their shapes and the resultant interactions is also important. A recent example of this approach is the application of MOCs **37–39** reported by Terenzi. These three Pt molecular squares of distinct sizes showed biological activity against cancer cells and heavily influenced the expression of genes known to form G-quadruplexes in their promoter regions. MOC-based molecular recognition will facilitate shape-related biomedical applications, which might be further used in treating other kinds of diseases. For example, MOC **110** recognizes proteins by its topological structure, MOC **116** recognizes L-dopa and D-penicillamine by its chiral cavity, and MOC **117** recognizes hormones by host–guest interactions. After the relationships among size, shape, functional groups, and activity are established, MOCs can advance towards further biochemical and biomedical applications. The construction of 3D MOCs with diverse metal centers and topological structures is another challenging area of research. Due to their controllable size and number of cavities, 3D MOCs could be very promising for drug delivery and other biomedical applications. However, it is also clear that a lot more research, testing and evaluation and clinical trials need to be done before any of these unique, large self-assembled systems maybe become usable drugs.

ACKNOWLEDGMENTS

Y.S. thanks the National Natural Science Foundation of China (21503185, 51573194), and the Priority Academic Program Development of Jiangsu Higher Education Institutions. P.J.S. thanks the NIH (grant R01-CA215157) for financial support.

Funding Sources

NIH (Grant R01-CA215157)

NSFC (21503185, 51573194)

REFERENCES

1. Sun Y; Chen C; Stang PJ Soft materials with diverse suprastructures via the self-assembly of metal−organic complexes. Acc. Chem. Res 2019, 52, 802–817. [PubMed: 30794371]
2. Cook TR; Stang PJ Recent developments in the preparation and chemistry of metallacycles and metallacages via coordination. Chem. Rev 2015, 115, 7001–7045. [PubMed: 25813093]
3. Smulders MMJ; Riddell IA; Browne C; Nitschke JR Building on architectural principles for three-dimensional metallosupramolecular construction. Chem. Soc. Rev 2013, 42, 1728–1754. [PubMed: 23032789]
4. Chakrabarty R; Mukherjee PS; Stang PJ Supramolecular coordination: self-Assembly of finite two- and three-dimensional ensembles. Chem. Rev 2011, 111, 6810–6918. [PubMed: 21863792]
5. Cook TR; Zheng Y-R; Stang PJ Metal–organic frameworks and self-assembled supramolecular coordination complexes: comparing and contrasting the design, synthesis, and functionality of metal–organic materials. Chem. Rev 2013, 113, 734–777. [PubMed: 23121121]
6. Bols PS; Anderson HL Template-directed synthesis of molecular nanorings and cages. Acc. Chem. Res 2018, 51, 2083–2092. [PubMed: 30156831]
7. Judge N; Wang L; Ho YYL; Wang Y Molecular engineering of metal-organic cycles/cages for drug delivery. Macromol. Res 2018, 26, 1074–1084.
8. Therrien B; Furrer J The biological side of water-soluble arene ruthenium assemblies. Adv. Chem 2014, 2014, 1–20.
9. Casini A; Woods B; Wenzel M The Promise of self-assembled 3D supramolecular coordination complexes for biomedical applications. Inorg. Chem 2017, 56, 14715–14729. [PubMed: 29172467]
10. Ahmad N; Younus HA; Chughtai AH; Verpoort F Metal–organic molecular cages: applications of biochemical implications. Chem. Soc. Rev 2015, 44, 9–25. [PubMed: 25319756]
11. Orhan E; Garci A; Riedel T; Soudani M; Dyson PJ Therrien B. Cytotoxic double arene ruthenium metalla-cycles that overcome cisplatin resistance. J Organomet. Chem 2016, 803, 39–44.
12. Vardhan H; Yusubovc M; Verpoort F Self-assembled metal–organic polyhedra: an overview of various applications. Coord. Chem. Rev 2016, 306, 171–194.
13. Wang W; Wang Y-X; Yang H-B Supramolecular transformations within discrete coordination-driven supramolecular architectures. Chem. Soc. Rev 2016, 45, 2656–2693. [PubMed: 27009833]
14. Ward MD; Hunter CA; Williams NH Coordination cages based on Bis(pyrazolylpyridine) ligands: structures, dynamic behavior, guest binding, and catalysis. Acc. Chem. Res 2018, 51, 2073–2082. [PubMed: 30085644]
15. Zhang D; Ronson TK; Nitschke JR Functional capsules via subcomponent self-assembly. Acc. Chem. Res 2018, 51, 2423–2436. [PubMed: 30207688]
16. Mari C; Pierroz V; Ferrari S; Gasser G Combination of Ru(II) complexes and light: newfrontiers in cancer therapy. Chem. Sci 2015, 6, 2660–2686. [PubMed: 29308166]
17. Zarra S; Wood DM; Roberts DA; Nitschke JR Molecular containers in complex chemical systems. Chem. Soc. Rev 2015, 44, 419–432. [PubMed: 25029235]
18. Chen L-J; Yang H-B; Shionoya M Chiral metallosupramolecular architectures. Chem. Soc. Rev 2017, 46, 2555–2576. [PubMed: 28452389]
19. Cook TR; Vajpayee V; Lee MH; Stang PJ; Chi K-W Biomedical and biochemical applications of self-assembled metallacycles and metallacages. Acc. Chem. Res 2013, 46, 2464–2474. [PubMed: 23786636]
20. Ahmedova A Biomedical applications of metallosupramolecular assemblies-structural aspects of the anticancer activity. Front. Chem 2018, 6, doi: 10.3389/fchem.2018.00620.
21. Zhou J; Zhang Y; Yu G; Crawley MR; Fulong CRP; Friedman AE; Sengupta S; Sun J; Li Q; Huang F; Cook TR Highly emissive self-Assembled BODIPY-platinum supramolecular triangles. J. Am. Chem. Soc 2018, 140, 7730–7736. [PubMed: 29787269]

22. Yao Y; Zhao R; Shi Y; Cai Y; Chen J; Sun S; Zhang W; Tang R 2D amphiphilic organoplatinum(II) metallacycles:their syntheses, self-assembly in water andpotential application in photodynamic therapy. Chem. Commun 2018, 54, 8068–8071.
23. Zhou Z; Jiangping Liu X; Rees TW; Wang H; Li X; Chao H; Stang PJ Heterometallic Ru–Pt metallacycle for two-photonphotodynamic therapy. Proc. Natl. Acad. Sci. U S A 2018, 115, 5664–5669. [PubMed: 29760069]
24. Jana A; Bhowmick S; Kumar S; Singh K; Garg P; Das N Self-assembly of Pt(II) based nanoscalar ionic hexagons and their anticancer potencies. Inorg. Chim. Acta 2019, 484, 19–26.
25. Schmitt F; Freudenreich J; Barry NPE; Juillerat-Jeanneret L; Süss-Fink G; Therrien B Organometallic cages as vehicles for intracellular release of photosensitizers. J. Am. Chem. Soc 2012, 134, 754–757. [PubMed: 22185627]
26. Gupta G; Denoyelle-Di-Muroa E; Mbakidi J-P; Leroy-Lhez S; Sol V; Therrien B Delivery of porphin to cancer cells by organometallic Rh(III) and Ir(III) metalla-cages. J. Org. Chem 2015, 787, 44–50.
27. Yu G; Cook TR; Li Y; Yan X; Wu D; Shao L; Shen J; Tang G; Huang F; Chen X; Stang PJ Tetraphenylethene-based highly emissive metallacageas a component of theranostic supramolecular nanoparticles. Proc. Natl. Acad. Sci. U S A 2016, 113, 13720–13725. [PubMed: 27856738]
28. Yu G; Yu S; Saha ML; Zhou J; , J.; Cook TR; 5, Yung BC; Chen J; Mao Z; Zhang F; Zhou Z; Liu Y; Shao L; Wang S; Gao C; Huang F; Stang PJ; Chen X A discrete organoplatinum(II) metallacage as amultimodality theranostic platform for cancer photochemotherapy. Nat. Commun 2018, 9:4335. [PubMed: 30337535]
29. Yu G; Zhu B; Shao L; Zhou J; Saha ML; Shi B; Zhang Z; Hong T; Li S; Chen X; Stang PJ Host −guest complexation-mediated codelivery of anticancer drug and photosensitizer for cancer photochemotherapy. Proc. Natl. Acad. Sci. U S A 2019, 116, 6618–6623. [PubMed: 30894484]
30. McNeill SM; Preston D; Lewis JEM; Knerr-Rupp ARK; Graham DO; Wright JR; Giles GI; Crowley JD Biologically active $[Pd_2L_4]^{4+}$quadruply-strandedhelicates: stability and cytotoxicity. Dalton Trans 2015, 44, 11129–11136. [PubMed: 25997516]
31. Zhang M; Li S; Yan X; Zhou Z; Saha ML; Wang Y-C; Stang PJ Fluorescent metallacycle-cored polymers via covalent linkage and their use as contrast agents for cell imaging. Proc. Natl. Acad. Sci. U S A 2016, 113, 11100–11105. [PubMed: 27647900]
32. Lewis JEM; Gavey EL; Cameron SA; Crowley JD Stimuli-responsive Pd_2L_4 metallosupramolecular cages: towards targeted cisplatin drug delivery. Chem. Sci 2012, 3, 778–784.
33. Woods B; Wenzel MN; Williams T; Thomas SR; Jenkins RL; Casini A Exo-functionalized metallacages as host-guest systems for the anticancer drug cisplatin. Front. Chem 2019, 7, doi: 10.3389/fchem.2019.00068.
34. Chan AK-W; Lam WH; Tanaka Y; Wong KM-C; Yam VW-W Multiaddressable molecular rectangles with reversible host–guest interactions: modulation of pH-controlled guest release and capture. Proc. Natl. Acad. Sci. U S A 2015, 112, 690–695. [PubMed: 25568083]
35. Preston D; Lewis JEM; Crowley JD Multicavity $[Pd_nL_4]^{2n+}$ cages with controlled segregated binding of different guests. J. Am. Chem. Soc 2017, 139, 2379–2386. [PubMed: 28110525]
36. Yuan M; Weisser F; Sarkar B; Garci A; Braunstein P; Routaboul L; Therrien B Synthesis and electrochemical behavior of a zwitterion-bridged metalla-cage. Organometallics 2014, 33, 5043–5045.
37. Bhat IA; Jain R; Siddiqui MM; Saini DK; Mukherjee PS Water-soluble Pd_8L_4 self-assembled molecular barrel as an aqueous carrier for hydrophobic curcumin. Inorg. Chem 2017, 56, 5352–5360. [PubMed: 28394128]
38. Xu W-Q; Fan Y-Z; Wang H-P; Teng J; Li Y-H; Chen C-X; Fenske D; Jiang J-J; Su C-Y Investigation of binding behavior between drug molecule 5-fluoraciland M_4L_4-Type tetrahedral cages: selectivity, capture, and release. Chem. Eur. J 2017, 23, 3542–3547. [PubMed: 28094459]
39. Han H; Räder AFB; Reichart F; Aikman B; Wenzel MW; Woods B; Weinmü M; Ludwig BS; Stefan Stürup S; Groothuis GMM; Permentier HP; Bischoff R; Kessler H; Horvatovich P; Casini

A Bioconjugation of supramolecular metallacages to integrin ligands for targeted delivery of cisplatin. Bioconjugate Chem 2018, 29, 3856–3865.

40. Furrer MA; Schmitt F; Wiederkehr M; Juillerat-Jeanneret L; Therrien B Cellular delivery of pyrenyl-arene ruthenium complexes by a water-soluble arene ruthenium metalla-cage. Dalton Trans 2012, 41, 7201–7211. [PubMed: 22506276]
41. Yue Z; Wang H; Bowers DJ; Gao M; Stilgenbauer M; Nielsen F; Shelley JT; Zheng Y-R Nanoparticles of metal–organic cages designed to encapsulate platinum-based anticancer agents. Dalton Trans 2018, 47, 670–674. [PubMed: 29257160]
42. Yue Z; Wang H; Li Y; Qin Y; Xu L; Bowers DJ; Gangoda M; Li X; Yang H-B; Zheng Y-R Coordination-driven self-assembly of a Pt(IV) prodrug-conjugated supramolecular hexagon. Chem. Commun 2018, 54, 731–734.
43. Zheng Y-R; Suntharalingam K; Johnstoneand TC; Lippard SJ Encapsulation of Pt(IV) prodrugs within a Pt(II) cage for drug delivery. Chem. Sci 2015, 6, 1189–1193. [PubMed: 25621144]
44. Sato S; Ikemi M; Kikuchi T; Matsumura S; Shiba K; Fujita M Bridging adhesion of a protein onto an inorganic surface using self-assembled dual-functionalized spheres. J. Am. Chem. Soc 2015, 137, 12890–12896. [PubMed: 26190770]
45. Mishra A; Ravikumar S; Song YH; Prabhu NS; Kim H; Hong SH; Cheon S; Noh J; Chi K-W A new arene–Ru based supramolecular coordination complex for efficient binding and selective sensing of green fluorescent protein. Dalton Trans 2014, 43, 6032–6040. [PubMed: 24390643]
46. Paul LEH; Therrien B; Furrer J Interactions of arene ruthenium metallaprisms with human proteins. Org. Biomol. Chem 2015, 13, 946–953. [PubMed: 25410522]
47. Yamashina M; Akita M; Hasegawa T; Hayashi S; Yoshizawa M A polyaromatic nanocapsule as a sucrose receptor in water. Sci. Adv 2017, 3, e1701126. [PubMed: 28875169]
48. Mendez-Arroyo J; d'Aquino AI; Chinen AB; Manraj YD; Mirkin CA Reversible and selective encapsulation of dextromethorphan and β-estradiol using an asymmetric molecular capsule assembled via the weak-link approach. J. Am. Chem. Soc 2017, 139, 1368–1371. [PubMed: 28094924]
49. Paul LEH; Therrien B; Furrer J Reactivity of hexanuclear ruthenium metallaprisms towards nucleotides and a DNA decamer. J. Biol. Inorg. Chem 2015, 20, 49–59. [PubMed: 25380991]
50. Garci A; Castor KJ; Fakhoury J; Do J-L; Trani JD; Chidchob P; Stein RS; Mittermaier AK; Friščić T; Sleiman H Efficient and rapid mechanochemical assembly of platinum(II) squares for guanine quadruplex targeting. J. Am. Chem. Soc 2017, 139, 16913–16922. [PubMed: 29058892]
51. Schmidt A; Hollering M; Drees M; Casini A; Kühn FE Supramolecular exo-functionalized palladium cages: fluorescent properties and biologicalactivity. Dalton Trans 2016, 45, 8556–8565. [PubMed: 27126799]
52. Grishagin IV; Pollock B; Kushal S; Cook TR; Stang PJ; Olenyuk BZ In vivo anticancer activity of rhomboidal Pt(II) metallacycles. Proc. Natl. Acad. Sci. U S A 2014, 111, 18448–18453. [PubMed: 25516985]
53. Walker MG; Jarman PJ; Gill MR; Tian X; Ahmad H; Reddy PAN; McKenzie L; Weinstein JA; Meijer AJHM; Battaglia G; Smythe CGW; Thomas JA A self-assembled metallomacrocycle singlet oxygen sensitizer for photodynamic therapy. Chem. Eur. J 2016, 22, 5996–6000. [PubMed: 27000412]
54. Jana A; Lippmann P; Ott I; Das N Self-assembly of flexible [2 + 2] ionic metallamacrocycles and their cytotoxicity potency. Inorg. Chim. Acta 2018, 471, 223–227.
55. Sun Y; Ding F; Zhou Z; Li C; Pu M; Xu Y; Zhan Y; Lu X; Li H; Yang G; Sun Y; Stang J, P. J. Rhomboidal Pt(II) metallacycle-based NIR-II theranostic nanoprobe for tumor diagnosis and image-guided therapy. Proc. Natl. Acad. Sci. U S A 2019, 116, 1968–1973. [PubMed: 30670648]
56. Gupta G; Kumar JM; Garci A; Nagesh N; Therrien B Exploiting natural products to build metalla-assemblies: the anticancer Activity of embelin-derived Rh(III) and Ir(III) metalla-rectangles. Molecules 2014, 116, 6031–6046.
57. Gupta G; Nowak-Sliwinska P; Herrero N; Dyson PJ; Therrien B Increasing the selectivity of biologically active tetranuclear arene ruthenium assemblies. J. Org. Chem 2015, 796, 59–64.

58. Gupta G; Das A; Park KC; Tron A; Kim H; Mun J; Mandal N; Chi K-W; Lee YC Self-assembled novel BODIPY-based palladium supramolecules and their cellular localization. Inorg. Chem 2017, 56, 4615–4621.
59. Mishra A; Jeong YJ; Jo J-H; Kang SC; Kim H; Chi K-W Coordination-driven self-assembly and anticancer potency studies of arene−ruthenium-based molecular metalla-rectangles. Organomettalics 2014, 33, 1144–1151.
60. Domarco O; Lötsch D; Schreiber J; Dinhof C; Van Schoonhoven S; García MD;. Peinador C; Keppler BK; Berger W; Terenzi A Self-assembled Pt_2L_2 boxes strongly bind G-quadruplex DNA and influence gene expression in cancer cells. Dalton Trans 2017, 46, 329–332. [PubMed: 27918050]
61. Bhowmick S; Jana A; Singh K; Gupta P; Gangrade A; Mandal BB; Das N Coordination-driven self-assembly of ionic irregular hexagonal metallamacrocycles via an organometallic clip and their cytotoxicity potency. Inorg. Chem 2018, 57, 3615–3625. [PubMed: 28841011]
62. Mishra A; Lee SC; Kaushik N; Cook TR; Choi EH; Kaushik NK; Stang PJ; Chi K-W Self-assembled supramolecular hetero-bimetallacycles for anticancer potency by intracellular release. Chem. Eur. J 2014, 20, 14410–14420. [PubMed: 25209962]
63. Ahmedova A; Momekova D; Yamashina M; Shestakova P; Momekov G; Akita M; Yoshizawa M Anticancer potencies of PtII-and PdII-linked M2L4 coordination capsules with improved selectivity. Chem. Asian. J 2016, 11, 474–477. [PubMed: 26629785]
64. Gupta G; Kumar JM; Garci A; Rangaraj N; Nagesh N; Therrien B Anticancer activity of half-sandwich RhIII and IrIII metalla-prisms containing lipophilic side chains. ChemPlusChem 2014, 79, 610–618.
65. Zheng Y-R; Suntharalingam K; Bruno PM; Lina W; Wang W; Hemann MT; Lippard SJ Mechanistic studies of the anticancer activity of an octahedral hexanuclear Pt(II) cage. Inorg. Chim. Acta 2016, 452, 125–129.
66. Mishra A; Jeong YJ; Jo J-H; Kang SK; Lah MS; Chi K-W Anticancer potency studies of coordination driven self-assembled arene–Ru-based metalla-bowls. ChemBioChem 2014, 15, 695–700. [PubMed: 24677392]
67. Singh N; Jang S; Jo J-H; Kim DH; Park DW; Kim I; Kim H; Kang SC; Chi K-W Coordination-driven self-assembly and anticancer potency studies of ruthenium–cobalt-based heterometallic rectangles. Chem. Eur. J 2016, 22, 16157–16164. [PubMed: 27689935]
68. Yu G; Zhang M; Saha ML; Mao Z; Chen J; Yao Y; Zhou Z; , Liu Y; Gao C; Huang F; Chen X; Stang PJ Antitumor activity of a unique polymer that incorporates a fluorescent self-assembled metallacycle. J. Am. Chem. Soc2017, 139, 15940–15949. [PubMed: 29019660]
69. Dubey A; Jeong YJ; Jo JH; Woo S; Kim DH; Kim H; Kang C; Stang PJ; Chi K-W Anticancer activity and autophagy involvement of self-assembled arene−ruthenium metallacycles. Organometallics 2015, 34, 4507–4514.
70. Gupta G; Das A; Ghate NB; Kim T; Ryu JY; Lee J; Mandal N; Lee CY Novel BODIPY-based Ru(II) and Ir(III) metalla-rectangles: cellular localization of compounds and their antiproliferative activities. Chem. Commun 2016, 52, 4274–4277.
71. Zhao Y; Zhang L; Li X; Shi Y; Ding R; Teng M; Zhang P; Cao C; Stang PJ Self-assembled ruthenium (II) metallacycles and metallacages with imidazole-based ligands and their in vitro anticancer activity. Proc. Natl. Acad. Sci. U S A 2019, 116, 4090–4098.
72. Adeyemo AA; Shettar A; Bhat IA; Kondaiah P; Mukherjee PS Self-assembly of discrete RuII8 molecular cages and their in vitro anticancer activity. Inorg. Chem 2017, 56, 608–617. [PubMed: 27997153]
73. Schmidt A; Molano V; Hollering M; Pçthig A; Casini A; Kühn FE Evaluation of new palladium cages as potential delivery systems for the anticancer drug cisplatin. Chem. Eur. J 2016, 22, 2253–2256. [PubMed: 26756963]
74. Kaiser F; Schmidt A; Heydenreuter W; Altmann PJ; Casini A; Sieber AA;. Kühn FE Self-assembled palladium and platinum coordination cages: photophysical studies and anticancer activity. Eur. J. Inorg. Chem 2016, 5189–5196.

75. Yi JW; Barry NPE; Furrer MA; Zava O; Dyson PJ; Therrien B; Kim BH Delivery of floxuridine derivatives to cancer cells by water-soluble organometallic cages. Bioconjugate Chem 2012, 23, 461–471.

76. Dattaa S; Misra SK; Saha ML; Lahiri N; Louie J; Pan D; Stang PJ Orthogonal self-assembly of an organoplatinum(II) metallacycle and cucurbit[8]uril that delivers curcumin to cancer cells. Proc. Natl. Acad. Sci. U S A 2018, 115, 8087–8092. [PubMed: 30038010]

77. Cullen W; Turega S; Hunter CA;. Ward MD pH-dependent binding of guests in the cavity of apolyhedral coordination cage: reversible uptake and release of drug molecules. Chem. Sci 2015, 6, 625–631. [PubMed: 28936311]

78. Du S; Yu T-Q; Liao W; Hu C Structure modeling, synthesis and X-ray diffraction determination of an extra-large calixarene-based coordination cage and its application in drug delivery. Dalton Trans 2015, 44, 14394–14402. [PubMed: 26200471]

79. Chen L-J; Ren Y-Y; Wu N-W; Sun B; Ma J-Q; Zhang L; Tan H; Liu M; Li X; Yang H-B Hierarchical self-assembly of discrete organoplatinum(II) metallacycles with polysaccharide via electrostatic interactions and their application for heparin detection. J. Am. Chem. Soc 2015, 137, 11725–11735. [PubMed: 26322626]

80. Dong J; Tan C; Zhang K; Liu Y; Low PJ; Jiang J; Cui Y Chiral NH-controlled supramolecular metallacycles. J. Am. Chem. Soc 2017, 139, 1554–1564. [PubMed: 28059502]

81. Tian Y; Yan X; Saha ML; Niu Z; Stang PJ Hierarchical self-assembly of responsive organoplatinum(II) metallacycle-TMV complexes with turn-on fluorescence. J. Am. Chem. Soc 2016, 138, 12033–12036. [PubMed: 27608138]

82. Wang H; Qian X; Wang K; Su M; Haoyang W; Jiang X; Brzozowski R; Wang M; Gao X; Li Y; Xu B; Eswara P; Hao X-Q; Gong W; Hou J-L; Cai J; Li X Supramolecular Kandinsky circles with high antibacterial activity. Nat. Commun 2018, 9:1815. [PubMed: 29739936]

83. Howson1 SE; Bolhuis A; Brabec V; Clarkson GJ; Malina J; Rodger A; Scott P Optically pure, water-stable metallo-helical 'flexicate' assemblies with antibiotic activity. Nat. Chem 2012, 4, 31–36.

84. Malina J; Scott P; Brabec V Recognition of DNA/RNA bulges by antimicrobial and antitumor metallohelices. Dalton Trans 2015, 44, 14656–14665. [PubMed: 26212708]

85. Richards AD; Rodger A; Hannon MJ; Bolhuis A Antimicrobial activity of an iron triple helicate. Int. J. Antimicrob. Agents 2009, 33, 469–472. [PubMed: 19157798]

86. Shi B; Liu Y; Zhu H; Vanderlinden R; T.; Shangguan L; Ni R; Acharyya K; Tang J-H; Zhou Z; Li X; Huang F; Stang PJ Spontaneous formation of a cross-linked supramolecular polymer both in the solid state and in solution, driven by platinum(II) metallacycle-based host−guest interactions. J. Am. Chem. Soc 2019, 141, 6494–6498. [PubMed: 30966741]

87. Sun Y; Zhang F; Jiang S; Wang Z; Ni R; Wang H; Zhou W; Li X; Stang PJ Assembly of metallacages into soft suprastructures with dimensions of up to micrometers and the formation of composite materials. J. Am. Chem. Soc 2018, 140, 17297–17307. [PubMed: 30424604]

88. Sun Y; Yao Y; Wang H; Fu W; Chen C; Saha ML; Zhang M; Datta S; Zhou Z; Yu H; Li X; Stang PJ Self-assembly of metallacages into multidimensional suprastructures with tunable emissions. J. Am. Chem. Soc 2018, 140, 12819–12828. [PubMed: 30212221]

89. Mannancherril V; Therrien B Strategies toward the enhanced permeability and retention effect by increasing the molecular weight of arene ruthenium metallassemblies. Inorg. Chem 2018, 57, 3626–3633. [PubMed: 29271651]

90. Preston D; McNeill SM; Lewis JEM; Giles GI; Crowley JD Enhanced kinetic stability of $[Pd_2L_4]_{4+}$cages through ligand substitution. Dalton Trans 2016, 45, 8050–8060. [PubMed: 27074828]

91. Han J; Schmidt A; Zhang T; Permentier H Groothuis GMM; Bischoff R; Kuhn FE; Horvatovich P; Casini A Bioconjugation strategies to couple supramolecular *exo*-functionalized palladium cages to peptides for biomedical applications. Chem. Commun 2017, 53, 1405–1408.

92. Fu Y; Romero MJ; Salassa L; Cheng X; Habtemariam A; Clarkson GJ; Prokes I; Rodger A; Costantini G; Sadler PJ Os_2 -Os_4 switch controls DNA knotting and anticancer activity. Angew. Chem. Int. Ed 2016, 55, 8909–8912.

93. Qin Y; Chen L-J; Dong F; Jiang S-T; Yin G-Q; Li X; Tian Y; Yang H-B Light-controlled generation of singlet oxygen within a discrete dual-stage metallacycle for cancer therapy. J. Am. Chem. Soc 2019, doi; 10.1021/jacs.9b026.

94. Hong CM; Kaphan DM; Bergmam RG; Raymond KN; Toste FD Conformational selection as the mechanism of guest binding in a flexible supramolecular host. J. Am. Chem. Soc 2017, 139, 8013–8021. [PubMed: 28581740]

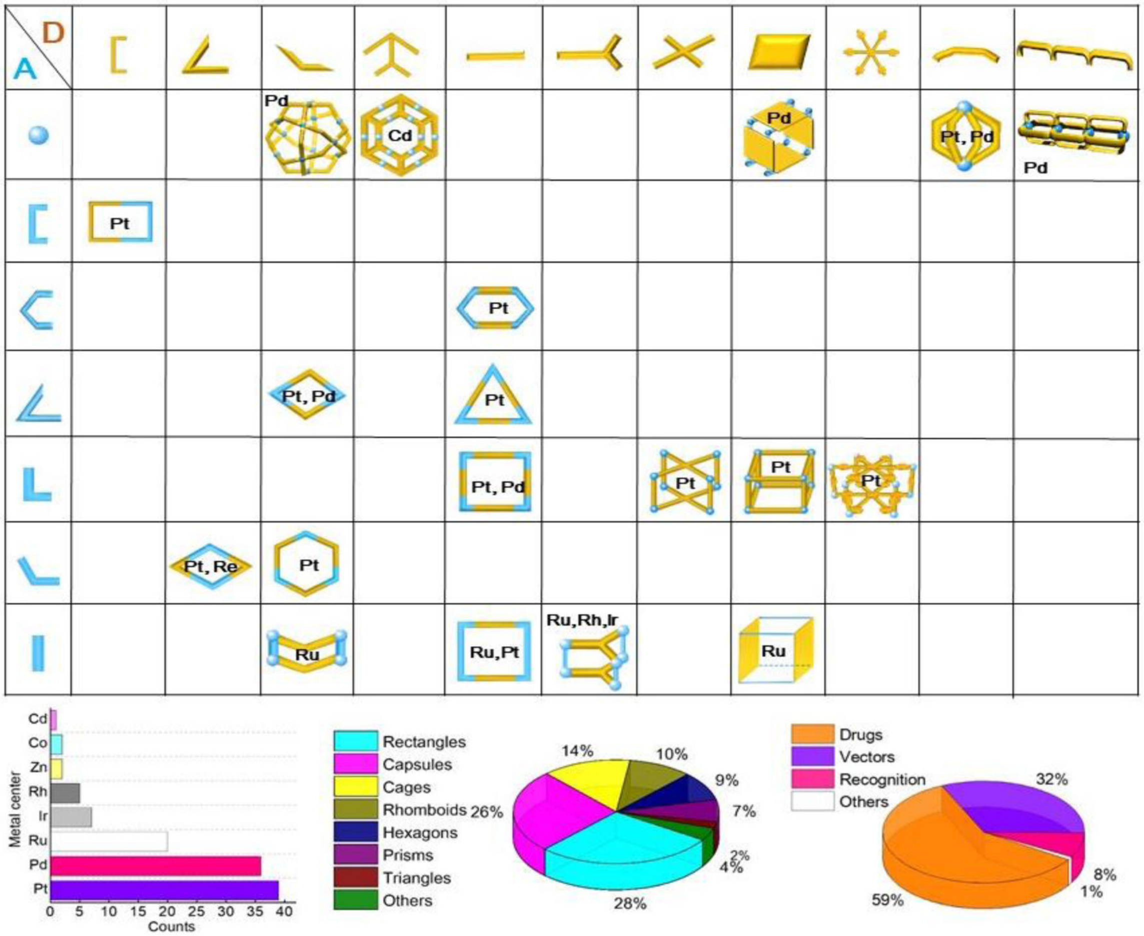

Scheme 1.

(Top) Diverse MOCs for biochemical and biomedical applications. (Bottom, left) Metal centers in MOCs for biomedical applications (Re, Cu and Mn containing heterometallic complexes are not counted). (Bottom, middle) Shape effect of various MOCs for biomedical applications. (Bottom, right) Different biological areas involving MOCs. Note: the statistical data is based on the selected 119 MOCs in this perspective.

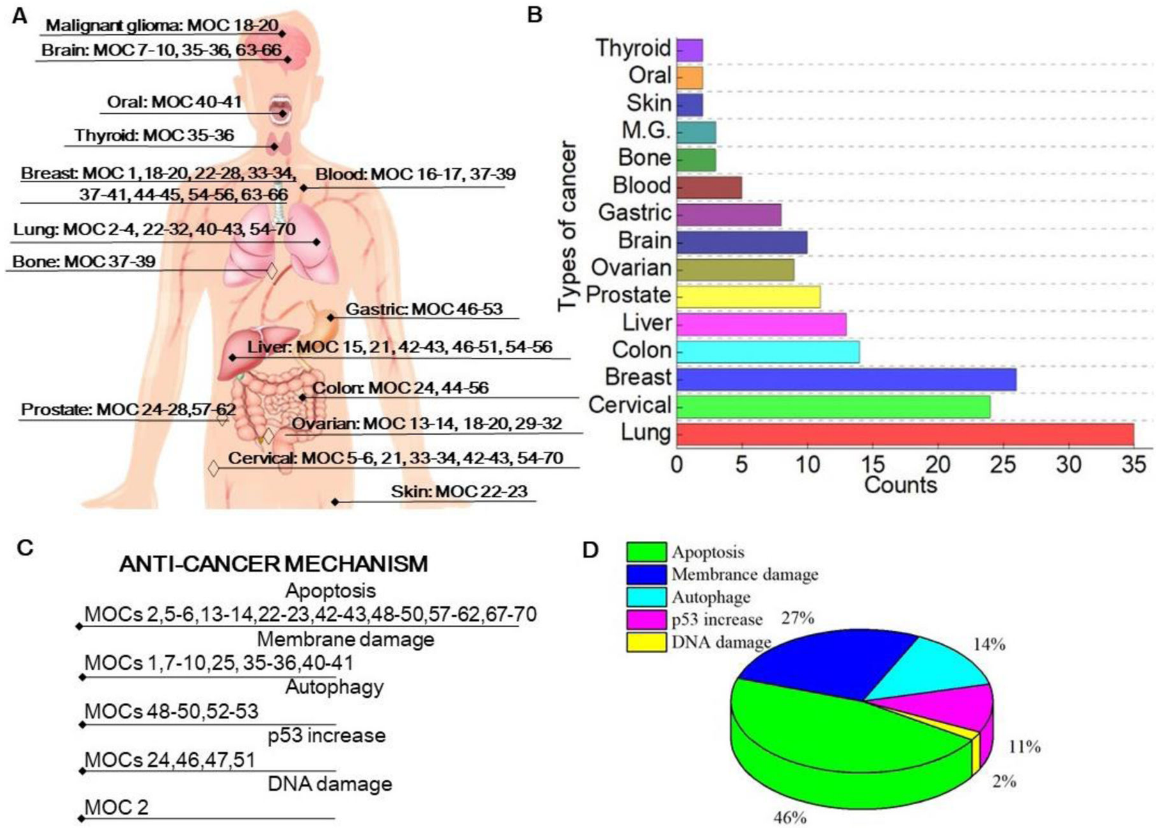

Scheme 2.

(A) The relationship between MOCs and target organs (M. G is the abbreviation of "malignant glioma". The target organ for "♦" \is demonstrated in the anatomical diagram, and not for "◊"). (B) The number of different MOCs in this perspective related to its targeted cancer type. (C) Anticancer mechanism (the statistical data is based on the mechanism that is mentioned in the original research paper). (D) Pie chart of anticancer mechanisms.

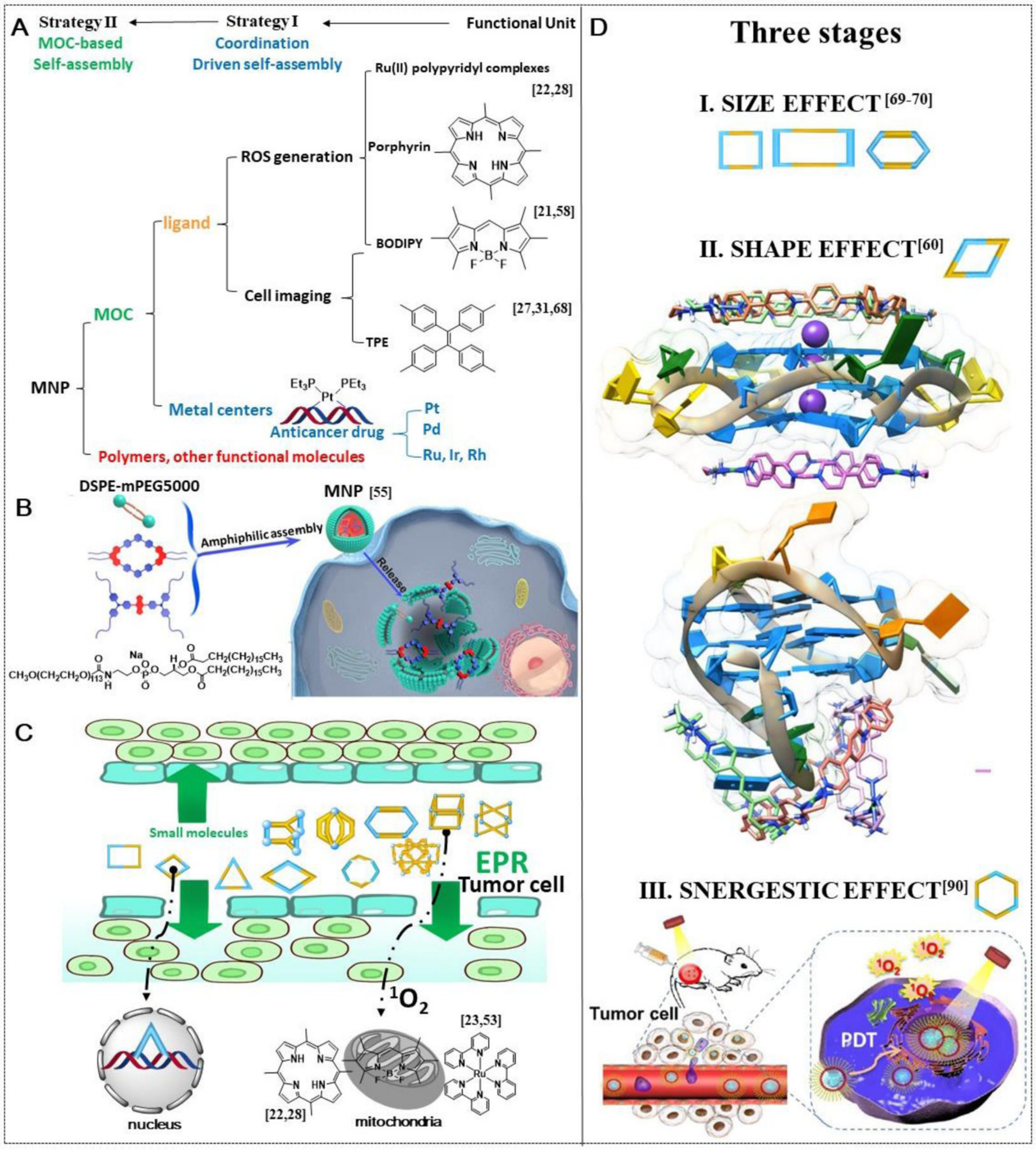

Scheme 3.

(A) Two strategies toward the construction of MOC based anticancer drugs. (B) MOCs used as coassembly units for construction MNPs. (C) MOCs uptake by cell due to EPR effect and the target organelles. (D) Three stages of MOCs based anticancer drugs, from size effect, to shape effect and then the synergistic effect. Adapted with permission from refs 21–23, 27–28, 31, 53–55, 57–60, 68 and 90. Copyright 2015, 2017, 2018 and 2019 American Chemical Society, 2017 and 2018 the Royal Society of Chemistry, 2016, 2018 and 2019 National Academy of Sciences (USA), 2016 Wiley-VCH, 2018 Elsevier. 2018 Nature Publishing Group.

Author Manuscript
Author Manuscript
Author Manuscript

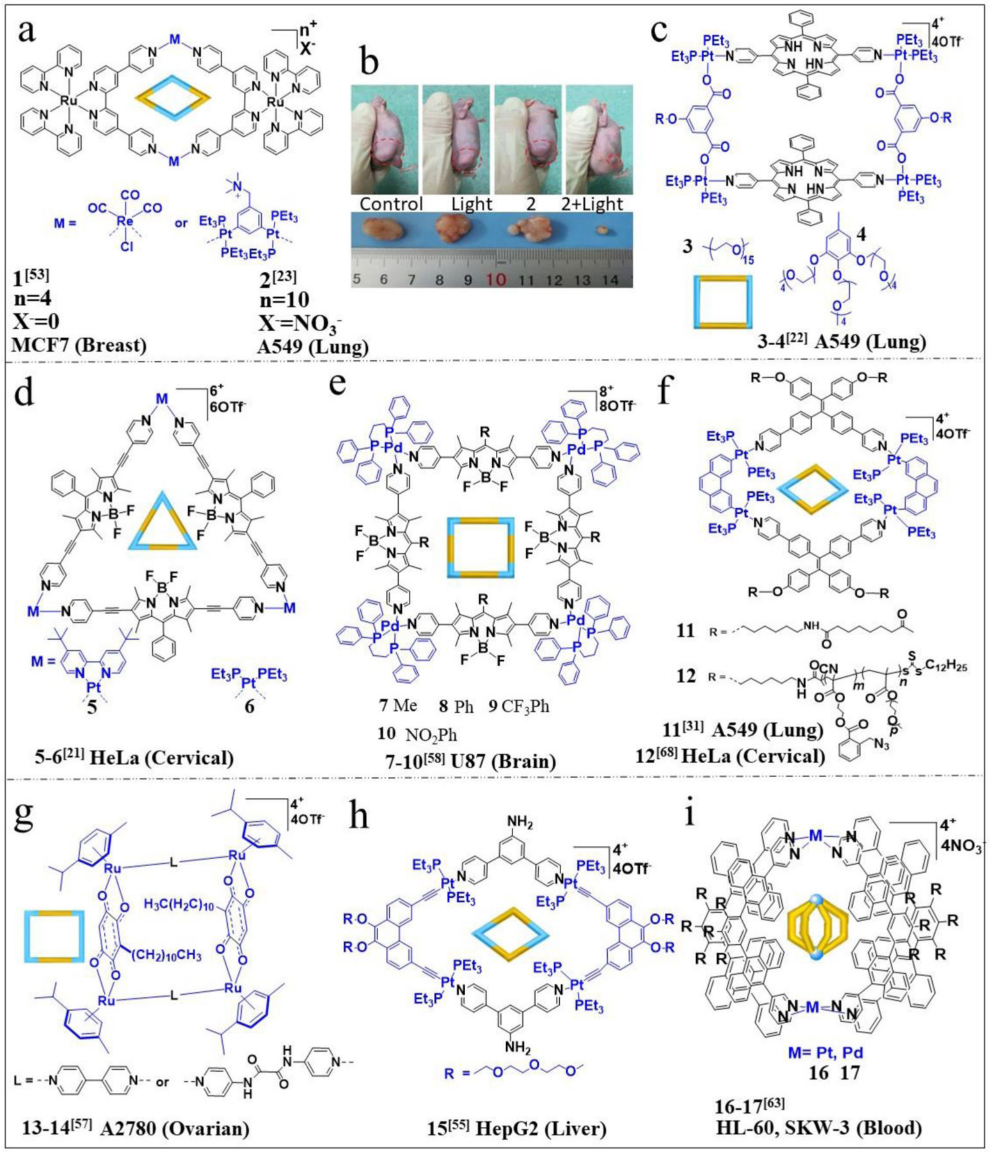

Figure 1.

Chemical structures of (a) MOCs **1–2**; (b) MOC **2**-related anticancer treatment. Chemical structures of (c) MOCs **3, 4**, (d) MOCs **5, 6**, (e) MOCs **7–10**, (f) MOCs **11, 12,** (g) MOCs **13, 14**, (h) MOC **15**, and (i) MOCs **16, 17**. Adapted with permission from refs 21–23, 31, 53, 55, 57, 58 and 63. Blue color refers metal containing acceptors, black color refers organic donors Copyright 2017 and 2018 American Chemical Society, 2018 the Royal Society of Chemistry, 2016, 2018 and 2019 National Academy of Sciences (USA), 2016 Wiley-VCH.

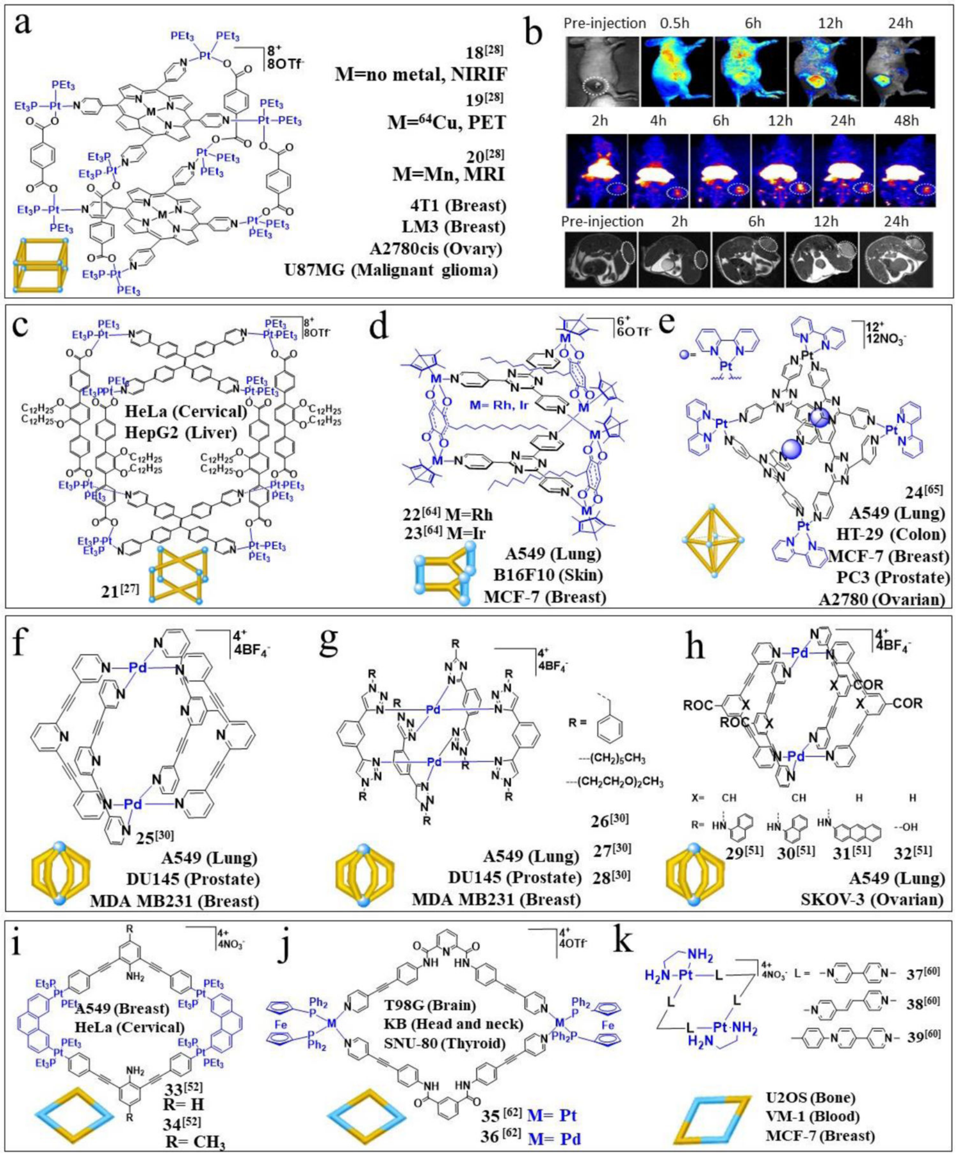

Figure 2.

(a) Chemical structures of MOCs **18–20**; (b) MOC **18–20**-related anticancer therapy. Top, NIRFI of U87MG tumor-bearing nude mice following injection of MNPs. Middle, PET image of U87MG tumor-bearing nude mice at 2, 4, 6, 12, 24, and 48 h post injection of 64Cu@MNPs. Bottom, in vivo T1-weighted axial MRI images (7T) of the mice before and after injection of Mn@MNPs. Chemical structures of (c) MOC **21**, (d) MOCs **22, 23**, (e) MOC **24**, (f) MOC **25**, (g) MOCs **26–28**, (h) MOCs **29–32**, (i) MOCs **33, 34**, (j) MOCs **35, 36**, and (k) MOCs **37–39**. Adapted with permission from refs 27–28, 30, 51–52, 60, 62 and 64–65. 2015, 2016 and 2017 the Royal Society of Chemistry, 2014 and 2016 National Academy of Sciences (USA), 2014 Wiley-VCH, 2016 Elsevier. 2018 Nature Publishing Group.

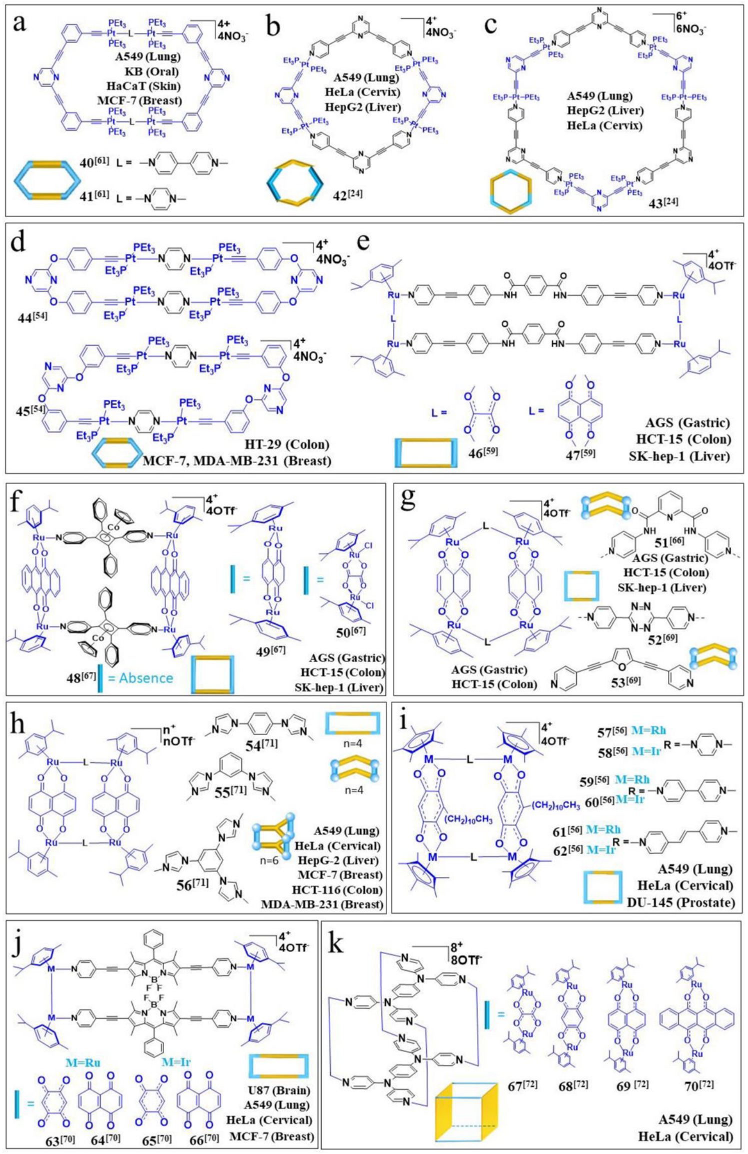

Figure 3.

Chemical structures of (a) MOCs **40, 41**, (b) MOC **42**, (c) MOC **43**, (d) MOCs **44, 45**, (e) MOCs **46, 47**, (f) MOCs **48–50**, (g) MOCs **51–53**, (h) MOCs **54–56**, (i) MOCs **57–62**, (j) MOCs **63–66**, and (k) MOCs **67–70.** Adapted with permission from refs 24, 54, 56, 59, 61, 66–67, 69, 70–72. Copyright 2014, 2015, 2017 and 2018 American Chemical Society, 2016 the Royal Society of Chemistry, 2019 National Academy of Sciences (USA), 2014 and 2016 Wiley-VCH, 2018 and 2019 Elsevier. 2014 MDPI.

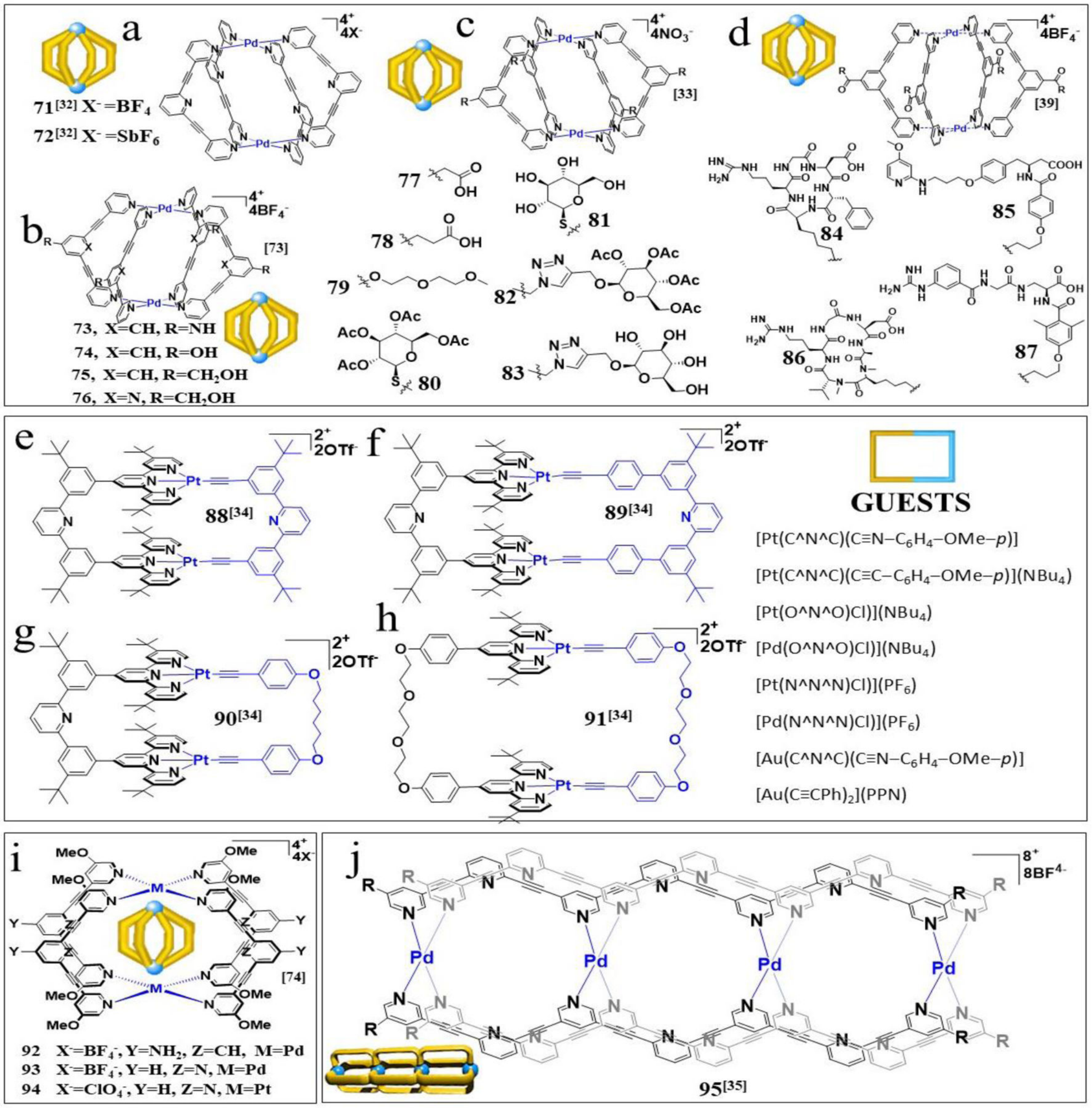

Figure 4.

Chemical structures of (a) MOCs **71, 72**, (b) MOCs **73–76**, (c) MOCs **77–83**, (d) MOCs **84–87**, (e) MOC **88**, (f) MOC **89**, (g) MOC **90**, (h) MOC **91**, inset, guests; (i) (a) MOCs **92–94**, and (j) MOC **95**. Adapted with permission from refs 32–35, 39 and 74. Adapted with permission from refs 32–35, 39 and 74. Copyright 2017 and 2018 American Chemical Society, 2012 the Royal Society of Chemistry, 2015 National Academy of Sciences (USA), 2016 Wiley-VCH, 2019 FRONTIERS MEDIA SA.

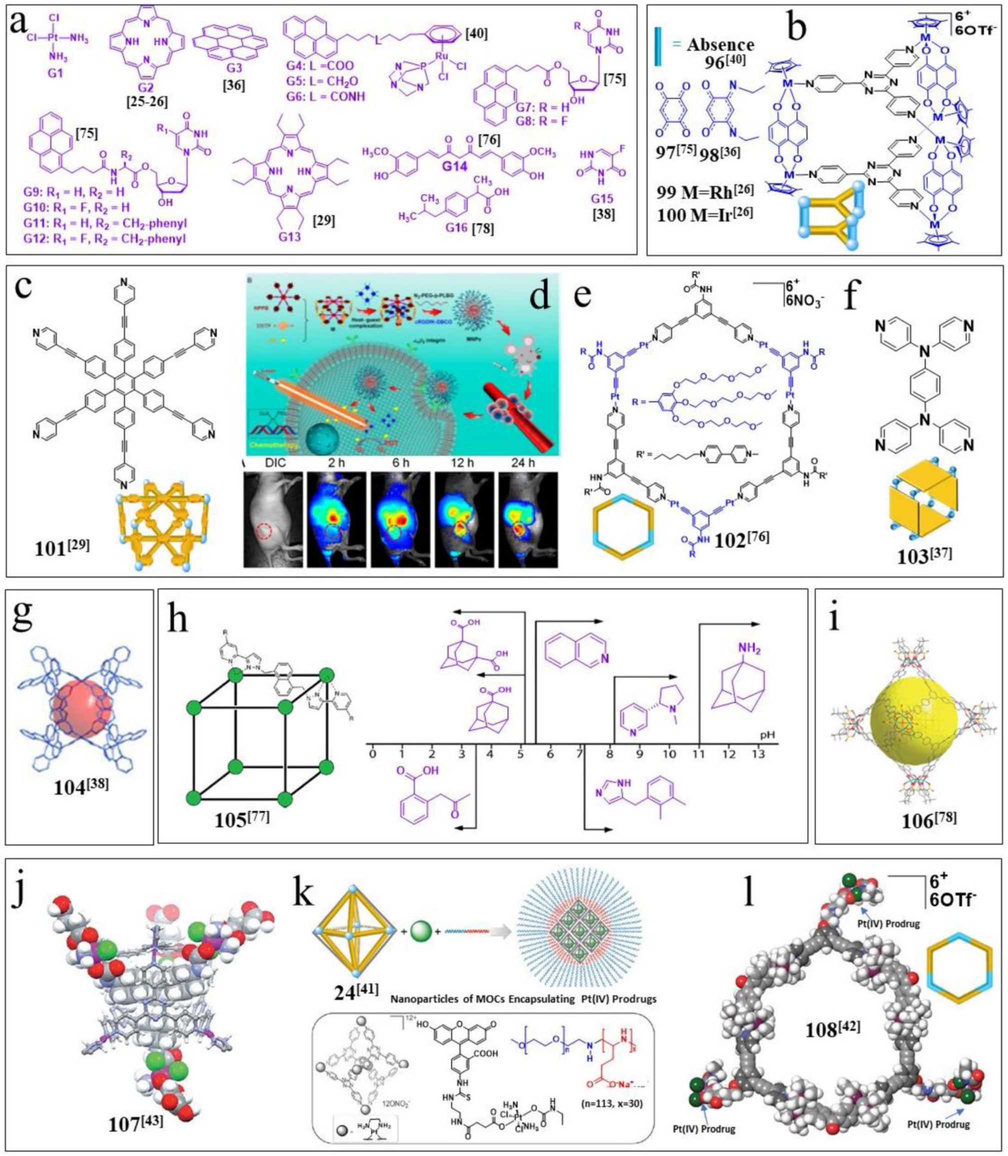

Figure 5.

Chemical structures of (a) guest molecules, (b) MOCs **96–100**, and (c) MOC **101**; (d) MOC **101**-related treatments. Chemical structures of (e) MOC **102**, (f) MOC **103**, (g) MOC **104**, (h) MOC **105**, (i) MOC **106**, (j) MOC **107**, (k) MOC **24 based MNP**, and (l) MOC **108**. Adapted with permission from refs 25–26, 29, 36–38, 40–43 and 75–78. Copyright 2012, 2014, 2015, 2017 American Chemical Society, 2012, 2015 and 2018 the Royal Society of Chemistry, 2018 and 2019 National Academy of Sciences (USA), 2017 Wiley-VCH.

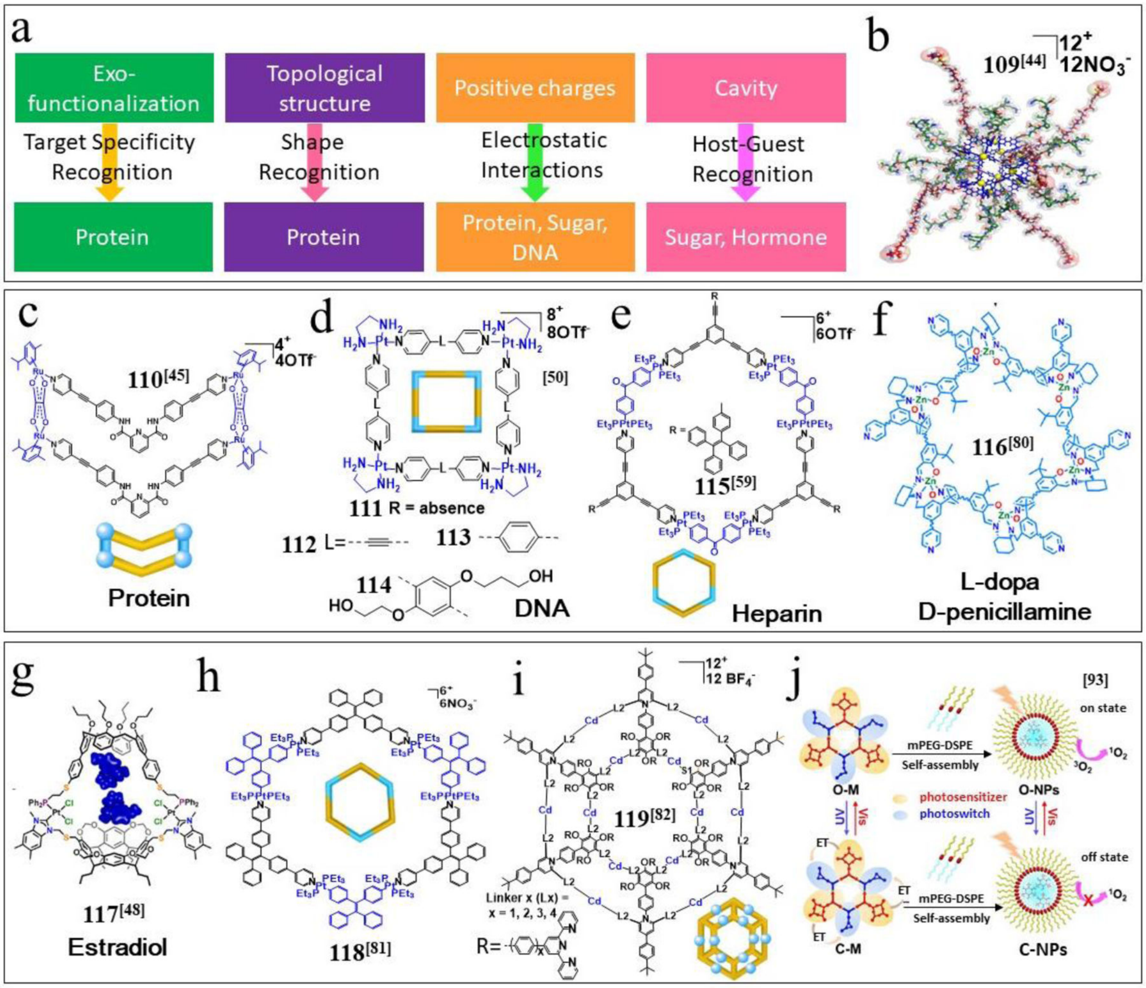

Figure 6.

(A) MOCs used for recognizing protein, sugar, DNA, hormone and the corresponding mechanism. Chemical structure of (b) MOC **109**, (c) MOC **110**, (d) MOCs **111–114**. (e) MOCs **115**, (f) MOC **116**, (g) MOC **117**, (h) MOC **118**, (i) MOC **119**, (j) schematic representation of the controllable generation of $^1O_2$ in metallacycle and nanoparticles.